

Old Dominion University

**ODU Digital Commons**

---

Electrical & Computer Engineering Faculty  
Publications

Electrical & Computer Engineering

---

1981

## **Slip Dislocation Formation During Continuous Wave Laser Annealing of Silicon**

Helmut Baumgart

Follow this and additional works at: [https://digitalcommons.odu.edu/ece\\_fac\\_pubs](https://digitalcommons.odu.edu/ece_fac_pubs)



Part of the [Electrical and Computer Engineering Commons](#), and the [Materials Science and Engineering Commons](#)

---

# Slip dislocation formation during cw laser annealing of silicon

H. Baumgart, F. Phillipp, G. A. Rozgonyi,<sup>a)</sup> and U. Gösele  
*Max-Planck-Institut für Festkörperforschung, and Max-Planck-Institut für Metallforschung,  
Heisenbergstrasse 1, D-7000 Stuttgart 80, Federal Republic of Germany*

(Received 6 August 1980; accepted for publication 29 October 1980)

High-voltage electron microscopy (HVEM) has been used for the investigation of the defect structure in cw laser-annealed silicon. We report for the first time a (HVEM) analysis of the formation processes involved in the nucleation and glide of slip dislocations during epitaxial regrowth by cw laser annealing of ion-implantation damaged silicon layers. Based on the combined optical and HVEM observations a model of the dislocation generation and glide processes is presented.

PACS numbers: 61.60.Jc, 79.20.Ds, 81.40.Ef, 61.70.Tm

The nucleation and propagation of dislocations in silicon has been an area of continued interest from both a fundamental and applied point of view for several decades. Recently, laser annealing has introduced several new elements into the modeling of dislocation phenomena due to the localized nature of the crystal heating and the extremely short times available for plastic flow phenomena to occur.<sup>1</sup> For example, following a pulsed laser melting, a surface will epitaxially regrow to a dislocation-free condition in less than 1  $\mu$  sec, while lattice strains as high as 1.5% are elastically frozen in.<sup>2</sup> However, cw laser annealing for several hundred milliseconds is generally accompanied by plastic flow in the form of slip dislocations and submicron dislocation loops.<sup>3,4</sup>

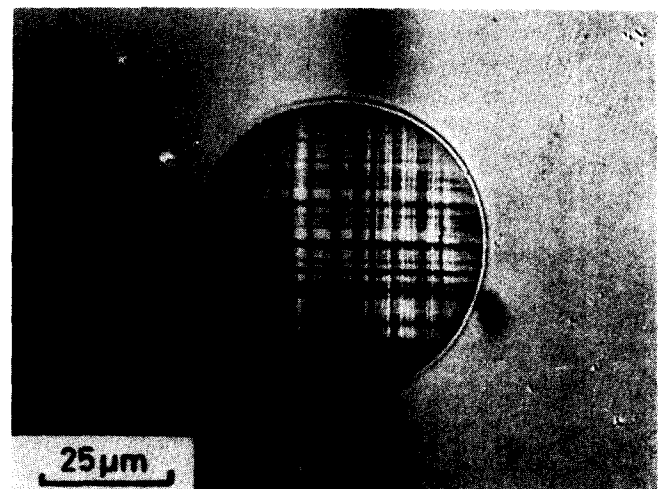
In the present letter, we report on a combined optical microscopy, etch pit, and high-voltage transmission electron microscopy (HVEM) study of dislocations deliberately introduced by a cw Ar-ion laser. The unique spatial, thermal, and temporal control of the laser-prepared samples, as well as the use of large-area thinning procedures provide new data, which has enabled us to formulate a model of the dislocation generation and glide processes.

Silicon specimens with  $\langle 100 \rangle$  orientation were amorphized by ion implantation of arsenic and silicon with doses ranging from  $1 \times 10^{15}$  to  $3 \times 10^{16}$   $\text{cm}^{-2}$  at 60 keV and subsequently laser irradiated. For comparison, virgin silicon wafers were also laser irradiated. A cw argon ion laser with a maximum output of 20 W was modified by insertion of an electromechanical shutter inside the laser cavity. In this way thermal "pulses" from 5 msec to several seconds could be directed at the sample. The specimen position was controlled by programmable  $xy$  stepping motors. Although a substrate table heatable to 500 °C is built into the system, no substrate heating was applied in the present study.

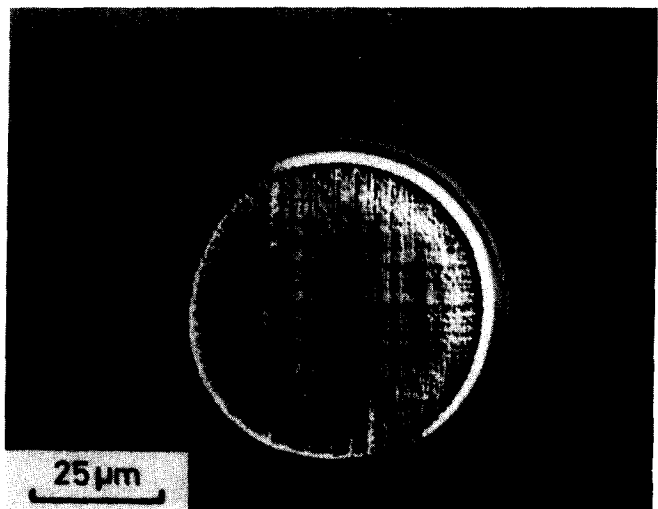
The laser-induced morphology changes were initially examined in a Nomarski differential interference contrast (DIC) microscope. Dislocation etch pits were produced by preferential chemical etching in the Secco solution.<sup>5</sup> Details of dislocation character and distribution were obtained in a Hitachi HU 650 high-voltage electron microscope operating at 600 keV. Large-area thinning produced foil thicknesses from 1 to 2  $\mu\text{m}$  over areas of several  $\text{mm}^2$ .<sup>6</sup> This technique

permitted the examination of several laser-irradiated spots of 50–80- $\mu\text{m}$  diameter from edge to edge and the comparison on a one-to-one basis with optical micrographs.

A typical slip line pattern revealed by DIC optical microscopy is shown in Fig. 1(a). The sample was As implanted and subsequently annealed via solid phase epitaxy, i.e., no melting has occurred. Note that the slip lines run from just



(a)



(b)

FIG. 1. Nomarski optical micrograph of solid-phase annealed silicon showing slip lines (a) as annealed and (b) Secco etched.

<sup>a)</sup>On sabbatical leave from Bell Laboratories, Murray Hill, N.J.

inside one edge of the annealed spot clear across the spot to just inside the opposite edge in two orthogonal  $\langle 110 \rangle$  directions. Although the slip lines travel essentially from edge to edge, etch pits are only observed in an annular region about  $10\text{-}\mu\text{m}$  wide, see Fig. 1(b). The absence of emerging dislocations in the center of a spot was confirmed in the HVEM by examination of an entire  $80\text{-}\mu\text{m}$ -diam laser-annealed spot, which indicated that the slip dislocations merely glide across the central region leaving behind surface slip traces.

Slip dislocations  $D_s$  and submicron dislocation loops  $D_1$  were found along the perimeter of spots as shown in Fig. 2(a). The slip dislocation consists of segments parallel to the surface and threading segments penetrating the  $1\text{-}2\text{-}\mu\text{m}$ -thick TEM specimen. The dislocation loops  $D_1$  (diameter  $\leq 100$  nm) were concentrated at the inner boundary of the defect-rich annular zone. Stereo pictures were used to establish the 3-dimensional configuration of the dislocations. The surface parallel segments  $p$  of the slip dislocations in Fig. 2(a) were found to be  $60^\circ$  dislocations with Burgers vector  $a/2 \langle 110 \rangle$  inclined to the specimen surface. The threading segments  $t$  of  $D_s$  are either screw or  $60^\circ$  dislocations. Detailed contrast analysis<sup>7</sup> of the small loops  $D_1$  proved them to be of interstitial type.

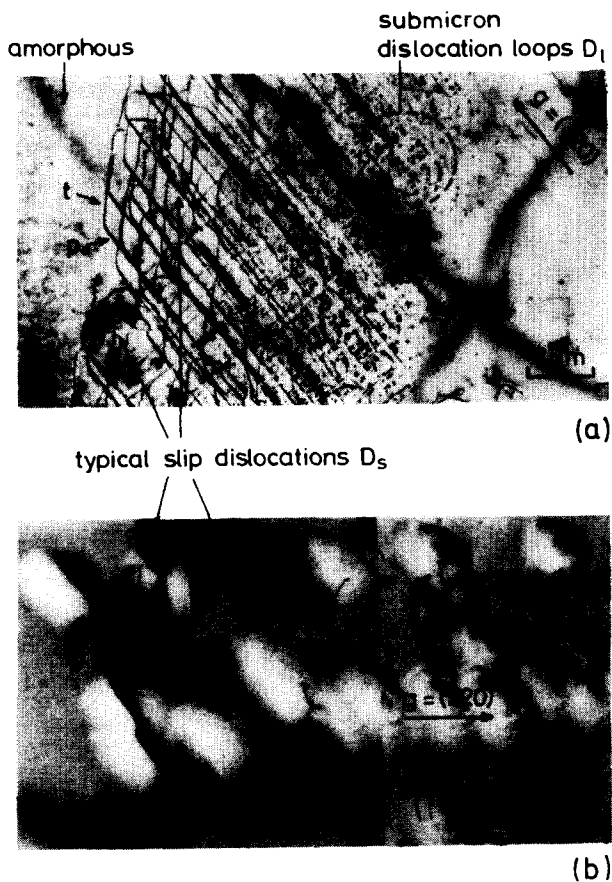


FIG. 2. High-voltage TEM micrograph of the periphery of irradiated areas; (a) as-implanted silicon, showing submicron dislocation loops  $D_1$ , dislocation segments parallel to the surface  $p$  and threading dislocation segments  $t$ , and (b) virgin silicon sample, showing pileup of threading dislocations.

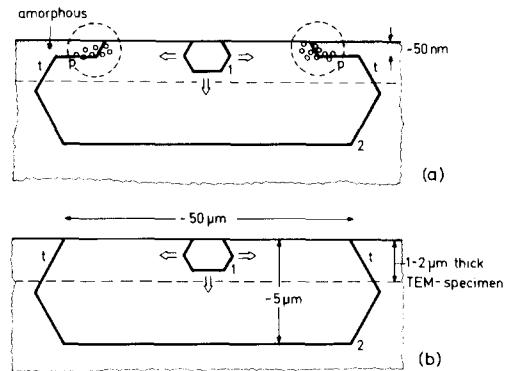


FIG. 3. Schematic of dislocation nucleation and subsequent glide in (a) implanted silicon, and (b) virgin silicon. 1: early stage of expanding half-loop, 2: final stage of expanding half-loop,  $p$ : dislocation segment parallel to the surface, and  $t$ : threading dislocation segment regions where submicron dislocation loops as observed are indicated by the broken circles.

The dislocation cross grid in Fig. 2(a) is typical for the defect structure observed after cw laser annealing irrespective of the species of ion implantation. Fig. 2(b) shows the dislocation structure obtained during a 200-msec pulse laser irradiation of virgin silicon wafers. No submicron loops or dislocation segments parallel to the surface could be seen. The slip dislocations show a simpler structure featuring only threading segments. Optical micrographs of virgin and implanted wafers are identical and appear as in Fig. 1(a) following laser irradiation.

These observations led us to the following model of generation and glide of dislocations in cw laser-annealed silicon: Lateral and in-depth temperature gradients are established during annealing. Mechanical stresses are therefore created by the localized expansion of the silicon lattice. Stress risers which naturally occur at the surface lead to the nucleation of dislocation half-loops.<sup>8</sup> Since the implanted surface is amorphous, the slip dislocations must nucleate after the solid phase epitaxial reconstruction of the amorphous layer has been completed. In fact, based on the time-dependent dislocation nucleation observations in Ref. 1 and also recently discussed in Ref. 4, the regrowth will always proceed to completion before the slip dislocations nucleate. Under the driving force of the asymmetrical, thermally induced mechanical stress, the dislocation half-loops expand by glide laterally and into the bulk as indicated in Fig. 3. Therefore these half-loops are *not* confined to the regrown layer depth of about 50 nm, but penetrate into the single-crystal substrate to a depth of about  $5\text{ }\mu\text{m}$ . The large loop penetration depth was determined during TEM foil preparation by appearance of a linear etch pattern due to the lower closing segment of the half-loops. Note that in Ref. 8 and also recently in Ref. 9, where similar generation mechanisms for dilatational-induced misfit dislocations are discussed, the depth of the half-loops is confined to the substrate/epi-layer<sup>8</sup> or substrate/dopant interface.<sup>9</sup>

In the case of ion-implanted samples the laterally expanding dislocation segments are pinned at the surface when they reach the boundary of the laser-irradiated area. The gliding dislocations are subsequently forced to expand below the partially annealed annular zone containing a high density of submicron dislocation loops at the inside edge of the

wedge-shaped<sup>3</sup> amorphous/single-crystal boundary. This process creates the dislocation segments  $p$ , seen in Fig. 2(a), which are parallel to the surface. Comparing the TEM micrograph with the schematic of Fig. 3(a) one has to bear in mind that the lower closing part of a dislocation half-loop is not contained in the TEM specimen.

The observation of pileups of dislocations lying in the same glide plane implies that multiplication processes do occur. Secondary sources leading to dislocation multiplication may be formed by cross slip of screw segments of the expanding half-loops.<sup>10,11</sup> The two rows of threading dislocations in Fig. 3(b) illustrate the pileup process in virgin silicon samples. Similar behavior is also found in the ion-implanted samples.

As outlined in the schematic of Fig. 3(b), the nucleation and glide mechanism in the virgin silicon samples is basically the same as in ion-implanted samples [Fig. 3(a)] but without the complication of dislocation pinning at the defect-rich outer annular zone.

In conclusion, we have presented the first high-voltage electron microscopy analysis of slip dislocations occurring during laser annealing of silicon. The large sample volume examined has enabled us to present a simple model for slip dislocation generation and glide mechanisms.

We gratefully acknowledge the help and support of M. Wilkens, H. J. Queisser, R. Uebbing, H. Strunk, D. Käss, and G. Packeiser. Part of this work has been supported under the technological program of the Federal Department of Research and Technology (BMFT) of the FRG.

<sup>1</sup>G. A. Rozgonyi and H. Baumgart, *J. de Physique* **41**, supplément 5, C-4-85 (1980)

<sup>2</sup>B. C. Larson, C. W. White, and B. R. Appleton, *Appl. Phys. Lett.* **32**, 801 (1978).

<sup>3</sup>G. A. Rozgonyi, H. J. Leamy, T. T. Sheng, and G. K. Celler, *Laser-Solid Interactions and Laser Processing*, in AIP Proceedings, edited by S. D. Ferris, H. J. Leamy, and J. M. Poate (AIP, New York, 1979), Vol. 50, p. 457.

<sup>4</sup>K. Ishida, H. Okabayashi, and M. Yoshida, *Appl. Phys. Lett.* **37**, 175 (1980).

<sup>5</sup>F. Secco D'Arragona, *J. Electrochem. Soc.* **119**, 948 (1972).

<sup>6</sup>B. O. Kolbesen, K. R. Mayer, and G. E. Schuh, *J. Phys. E* **8**, 197 (1975).

<sup>7</sup>H. Föll and M. Wilkens, *Phys. Status Solidi A* **31**, 519 (1975).

<sup>8</sup>J. W. Matthews, S. Mader, and T. B. Light, *J. Appl. Phys.* **41**, 3800 (1970).

<sup>9</sup>J. Narayan, B. C. Larson, and W. H. Christie, *Laser-Solid Interactions and Laser Processing 1978*, in AIP Conference Proceeding, edited by S. D. Ferris, H. J. Leamy, and J. M. Poate, (1979), Vol. 50, p. 440.

<sup>10</sup>M. Sato and K. Sumino, *High-Voltage Electron Microscopy, 1977* (Jap. Soc. of Electron Microscopy, Tokyo, 1977).

<sup>11</sup>W. Hagen and H. Strunk, *Appl. Phys.* **17**, 85-87 (1978).

## Internal photoemission in the anodic oxide/GaAs interface

S. Yokoyama, M. Hirose, and Y. Osaka

*Department of Electrical Engineering, Hiroshima University, Hiroshima 730, Japan*

T. Sawada and H. Hasegawa

*Department of Electrical Engineering, Hokkaido University, Sapporo 060, Japan*

(Received 18 August 1980; accepted for publication 28 October 1980)

The barrier height at the anodic oxide/GaAs interface has been determined by internal photoemission of the metal-oxide-semiconductor structures. The height of the potential barrier between the oxide and GaAs is found to be  $2.62 \pm 0.05$  eV for as-grown and  $2.39 \pm 0.05$  eV for hydrogen-annealed specimens. Quantum yield below the photoemission threshold is interpreted in terms of electron emission from interface states at energies above midgap of GaAs.

PACS numbers: 79.60.Eq, 73.40.Qv, 73.20.Hb, 73.60.Hy

Insulating oxides formed on GaAs by anodization<sup>1</sup> are potentially used for application to metal-oxide-semiconductor (MOS) technology, surface passivation, and metal-insulator-semiconductor (MIS) solar cells. A common feature of compound semiconductor MOS systems is anomalous behavior in their capacitance and conductance. For better understanding of such electrical anomalies, Hasegawa and Sawada<sup>2</sup> have recently proposed the interface-state-band (ISB) model for GaAs MOS structures and justified the model by a quantitative analysis of transient capacitance and deep level transient spectroscopy (DLTS) measurements. They assumed the barrier height at the oxide/GaAs interface being about 1.0 eV.<sup>3</sup> Further examination of this barrier height is needed to settle or improve the ISB model.

In this letter, we report the first observation of internal photoemission from GaAs to anodic oxide and the direct determination of the barrier height at the oxide/GaAs interface. Also, an analysis of photoemission spectra has revealed the presence of a high density of interface states above midgap of GaAs.

GaAs(100) wafers with carrier concentration of  $5.9 \times 10^{17}$  cm<sup>-3</sup> ( $n$  type) and  $1.0 \times 10^{18}$  cm<sup>-3</sup> ( $p$  type) were used as substrates, which were oxidized by a mixture of propylene glycol and buffered (3%) aqueous solution of tartaric acid. Anodization in the constant current mode at 0.5 mA/cm<sup>2</sup> was followed by the constant voltage mode at 190 V. The postgrowth annealing was carried out at 300 °C for 1.5 h in a hydrogen atmosphere. Finally, semitransparent